Available online at www.sciencedirect.com

SciVerse ScienceDirect

Energy Procedia 15 (2012) 30 – 39

Energy Procedia

International Conference on Materials for Advanced Technologies 2011, Symposium O

Advances in the Surface Passivation of Silicon Solar Cells

J. Schmidt[a,b,*], F. Werner[a], B. Veith[a], D. Zielke[a], S. Steingrube[a,b], P. P. Altermatt[a,b], S. Gatz[a], T. Dullweber[a] and R. Brendel[a,b]

[a] *Institute for Solar Energy Research Hamelin (ISFH), Am Ohrberg 1, 31860 Emmerthal, Germany*
[b] *Dep. Solar Energy, Institute of Solid-State Physics, Leibniz University of Hannover, Appelstr. 2, 30167 Hannover, Germany*

Abstract

The surface passivation properties of aluminium oxide (Al_2O_3) on crystalline Si are compared with the traditional passivation system of silicon nitride (SiN_x). It is shown that Al_2O_3 has fundamental advantages over SiN_x when applied to the rear of *p*-type silicon solar cells as well as to the p^+ emitter of *n*-type silicon solar cells. Special emphasis is paid to the transfer of Al_2O_3 into industrial solar cell production. We compare different Al_2O_3 deposition techniques suitable for mass production such as ultrafast spatial atomic layer deposition, inline plasma-enhanced chemical vapour deposition and reactive sputtering. Finally, we review the most recent cell results with Al_2O_3 passivation and give a brief outlook on the future prospects of Al_2O_3 in silicon solar cell production.

Keywords: Silicon; solar cells; surface passivation; aluminium oxide

1. Introduction

The most important advancement in the area of surface passivation of silicon solar cells in recent years was the re-introduction of aluminium oxide (Al_2O_3) [1-3]. As its properties are fundamentally different from that of other dielectric materials frequently used for the surface passivation of silicon solar cells – such as silicon nitride (SiN_x) or silicon dioxide (SiO_2) – Al_2O_3 fills a hitherto open gap in silicon-based photovoltaic technology. One major difference to most other dielectric passivation layers applied so far in photovoltaics – which usually contain a fixed positive charge density – is that Al_2O_3 contains a high density of fixed negative charges [1]. As a consequence, it shows a negligible injection level dependence

* Corresponding author. Tel.: +49 5151 999 100; fax: +49 5151 999 400
E-mail address: j.schmidt@isfh.de

doi:10.1016/j.egypro.2012.02.004

of the effective surface recombination velocity on *p*-type silicon [3] and it also prevents any parasitic shunting at the rear of locally contacted and passivated *p*-type silicon solar cells [4]. The negative fixed charge density in combination with a relatively low interface state density also provides the best passivation achieved to date on boron-diffused p^+-emitters as well as screen-printed Al-p^+ emitters for *n*-type silicon solar cells [5, 6]. Hence, today the surface passivation of silicon solar cells by Al_2O_3 is considered a key technology in future industrial high-efficiency solar cell production.

The first study of the surface passivation properties of Al_2O_3 on silicon was in fact already published in 1989 by Hezel and Jaeger [1]. They used the relatively simple deposition technique of atmospheric pressure chemical vapour deposition (APCVD) and demonstrated a very good level of surface passivation on *p*-type silicon. The reported fixed negative charge density of $Q_f = -3\times10^{12}$ cm^{-2} lies within the range of typical Q_f values of present-day well-passivating Al_2O_3 layers [7]. Hezel and Jaeger did not, however, measure the effective surface recombination velocity S_{eff}, which is a figure of merit that includes the effects of chemical as well as field-effect passivation. Instead, they reported the surface recombination velocity parameter S_0, which only includes the chemical interface passivation, to be at 210 cm/s. Considering the high negative Q_f value of the films we conjecture that Hezel and Jaeger already achieved S_{eff} values well below 100 cm/s on 2 Ωcm *p*-type silicon. In the following two decades this important result was however buried in oblivion until in 2006 Al_2O_3 was re-discovered as dielectric passivation layer for silicon solar cells [2, 3]. Agostinelli *et al.* [2] reported that thermal atomic-layer-deposited (ALD) Al_2O_3 layers provide effective surface recombination velocities S_{eff} below 100 cm/s on 2 Ωcm *p*-type Cz-Si. Later the same year Hoex *et al.* [3] reported that plasma-assisted atomic-layer-deposited (PA-ALD) Al_2O_3 is capable of providing an S_{eff} value of 13 cm/s on 2 Ωcm *p*-type FZ-Si and S_{eff} = 2 cm/s on 2 Ωcm *n*-type Cz-Si. It should be noted that their $S_{eff}(\Delta n)$ measurements showed a very weak injection dependence for the *p*-type wafers and a more pronounced dependence for the *n*-type wafers – which is, as shown in later studies, a fundamental property of the silicon surface passivation by negative-charge-dielectrics [8]. In the following year, the important finding was published that Al_2O_3 deposited by PA-ALD provides a hitherto unreached and stable level of surface passivation on boron-diffused p^+ emitters, where emitter saturation current densities J_{0e} in the order of 10-30 fA/cm^2 were achieved [5]. This was a major advancement compared to previously used passivation layers, such as thermally grown SiO_2, which is typically not long-term stable on boron-diffused p^+ emitters [9], and plasma-enhanced chemical vapour deposited (PECVD) SiN_x, which has problems concerning the passivation of highly doped *p*-type surfaces [10].

In this contribution, we focus on the fundamental differences between the silicon surface passivation by Al_2O_3 and the more traditional passivation layer SiN_x. Special emphasis is also paid to the transfer of Al_2O_3 into industrial solar cell production. This is a crucial point, as the conventional ALD deposition systems are not compatible with the high throughput required in solar cell production. Hence, we compare different Al_2O_3 deposition techniques suitable for mass production such as high-rate spatial ALD, PECVD and sputtering. Finally, we will summarise the latest results concerning lab-type small-area silicon solar cells as well as industrial-type large-area cells.

2. Negatively charged vs. positively charged dielectrics: Al_2O_3 vs. SiN_x

The surface passivation properties of dielectric layers depend crucially on the fixed charge density Q_f in the dielectric layer or at the interface, which will be discussed in more detail below. The most frequently used dielectric in photovoltaics is SiN_x deposited by PECVD. During deposition onto a silicon wafer, electrons are transferred from the growing SiN_x layer into the energetically favourable silicon

wafer. The positive charges extend about 20 nm into the SiN_x [11]. As a consequence, the field-effect passivation level provided by the fixed positive charges within the SiN_x increases until a SiN_x layer thickness of about 20 nm is reached. Note that an introduction of a SiO_2 layer between the Si wafer and the SiN_x layer hampers the charge transfer from the SiN_x into the Si and completely eliminates the charge transfer above a crucial thickness of about 5 nm. The SiO_2 layer itself also contains positive charges, however, they are typically well below the Q_f values detected in single SiN_x layers [12]. Deposition of Al_2O_3 leads already during the growth of the first nanometer to the formation of a large amount of negative charges. For Al_2O_3 on Si it has been shown that the charges are located extremely close to the interface [13, 14]. The nature of the charged defects within the two different dielectric layers seems to be fundamentally different. In the case of SiN_x the charged defects are homogeneously distributed throughout the bulk of the layer. The positively charged defects are microscopically assigned to silicon dangling bonds which are back-bonded to three nitrogen atoms, the so-called K^+ centres [15, 16]. In the case of Al_2O_3 on Si, the microscopic origin of the negative charges is still under discussion. An ultrathin SiO_x layer (up to ~1 nm) has been detected in some studies, which was conjectured to play a crucial role in the formation of the negative Q_f [7]. In our samples, however, the SiO_x interfacial layer was found to be only a few monolayers thick and we detected instead a highly non-stoichiometric very oxygen-rich AlO_x within the first nanometer to the interface [14]. As Al vacancies and O interstitials are known to be negatively charged in aluminium oxide [17], we suggest that this non-stoichiometric AlO_x layer is the reason for the large negative Q_f detected close to the Si interface [14].

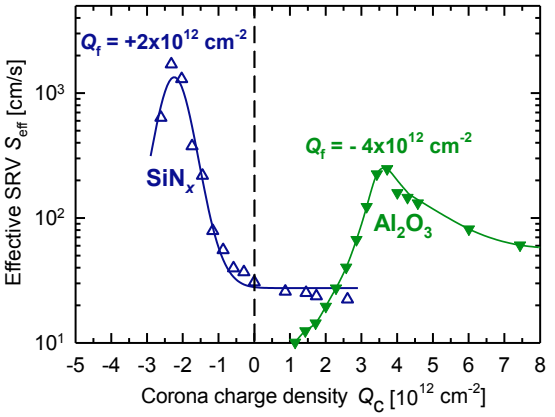

Fig. 1. Measured effective surface recombination velocity (SRV) S_{eff} as a function of the Corona charge density Q_C deposited onto PECVD-SiN_x and PA-ALD-Al_2O_3-coated 1-Ωcm *p*-type FZ Si wafer. The lines are guides to the eye.

Figure 1 shows a measurement of the effective surface recombination velocity (SRV) S_{eff} as a function of the Corona charge density Q_C deposited onto dielectric passivation layers of SiN_x and Al_2O_3. In the flatband case when $Q_C = -Q_f$, the recombination rate and hence $S_{eff}(Q_C)$ shows a maximum. As has been shown by Dauwe *et al.* [18], a hypothetical asymmetry in the capture cross sections for holes and electrons of the interface states has a negligible influence on the peak position. From the peak position the fixed charge density Q_f within the dielectric layer can hence be directly deduced. Figure 1 shows typical Corona-lifetime measurements for PECVD-SiN_x and PA-ALD-Al_2O_3 layers deposited onto 1-Ωcm *p*-type FZ Si wafers, where the deposited amount of charges has been determined via successive Kelvin probe measurements. The S_{eff} values were deduced from the effective lifetimes, which were measured by the quasi-steady-state photoconductance (QSSPC) technique [18]. As can be seen from Fig. 1, the fixed charge density within the SiN_x layer is positive and amounts to $Q_f = +2\times10^{12}$ elementary charges/cm^2, whereas the fixed charge density within the Al_2O_3 layer is negative and amounts to $Q_f = -4\times10^{12}$ cm^{-2}.

These are typical values for the respective dielectric passivation layers on silicon. The fixed negative charge density within the Al_2O_3 layer induces an accumulation layer at the *p*-type silicon surface in contrast to the SiN_x layer inducing and inversion layer. As will be shown below, this has a significant impact on the $S_{eff}(\Delta n)$ dependence provided by the two different dielectric materials, which is much weaker on *p*-Si in the case of Al_2O_3 passivation compared to SiN_x passivation (see Fig. 2). In addition, due to the formation of an accumulation layer instead of an inversion layer at the *p*-type silicon surface, the above-mentioned parasitic shunting effect at the solar cell rear does not occur for an Al_2O_3-rear-passivated cell [4]. Al_2O_3 is hence an optimal choice for the rear passivation of *p*-type silicon solar cells.

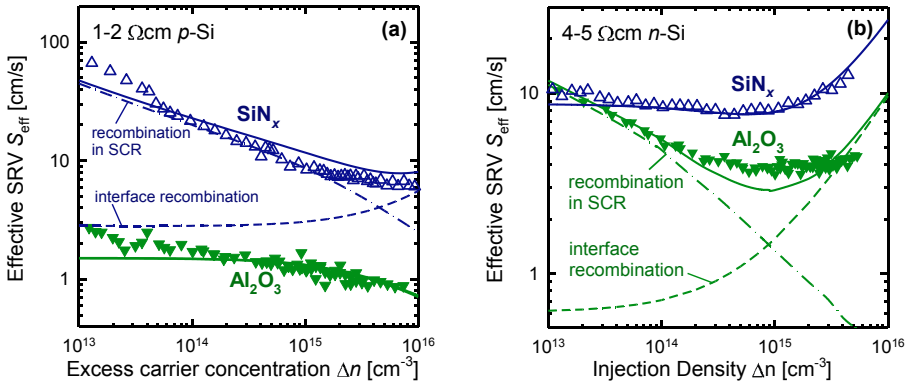

Fig. 2. Measured (symbols) and calculated (lines) $S_{eff}(\Delta n)$ dependence of PECVD-SiN_x and PA-ALD-Al_2O_3-passivated (a) *p*-type silicon and (b) *n*-type silicon. The pronounced injection-level dependence of S_{eff} at low Δn for SiN_x in *p*-type silicon and Al_2O_3 in *n*-type silicon is assigned to an enhanced recombination in the space charge region (SCR).

In order to model the $S_{eff}(\Delta n)$ dependence at the Si/SiO_2 interface, the so-called Girisch model [19] has been successfully applied in the past [12]. The only recombination channel considered in this model is recombination via interface states. The model is based on the Shockley-Read-Hall (SRH) equation and includes the effect of band bending in the silicon towards the interface due to the presence of charges in the SiO_2 and at the interface. In the case of SiN_x, where the band bending is much more pronounced compared to SiO_2 due to the more than one order of magnitude higher fixed positive charge density Q_f, it turned out that a modelling of the $S_{eff}(\Delta n)$ dependence is difficult using the simple Girisch approach. Due to the high Q_f of around $+2\times10^{12}$ elementary charges/cm^2 the Girisch model results in a negligible $S_{eff}(\Delta n)$ dependence (dashed line in Fig. 2(a)). The measurements on *p*-type silicon, however, typically show an increasing S_{eff} with decreasing Δn [16] (triangles up in Fig. 2(a)), a problematic behaviour for solar cell applications, as solar cells operate under various illumination conditions. It turned out, however, that assuming a surface-damaged region (SDR) of reduced lifetime in the silicon close to the interface (~100 nm) explains the observed behaviour. Due to the positive Q_f in the SiN_x layer, the SDR lies directly within the space charge region (SCR) and hence produces a significant contribution to the total recombination [20, 21]. The pronounced injection-level dependence of S_{eff} measured on SiN_x-passivated *p*-type silicon can hence mainly be attributed to recombination in the SCR (see dash-dotted line in Fig. 2(a)). The lines in Fig. 2 show calculated $S_{eff}(\Delta n)$ curves using the Girisch model and adding a SRH recombination channel within the SCR [20, 21]. More recently, Steingrube et al. [22] refined the model and were thereby able to consistently model the $S_{eff}(\Delta n)$ dependence of a broad variety of SiN_x-passivated *p*- and *n*-type silicon wafers of different resistivities. Importantly, as SiN_x produces no inversion layer, but an accumulation layer on *n*-type silicon, virtually no injection dependence is measured on *n*-type silicon, which is also in excellent agreement with the assumption of the presence of an SDR (triangles up in Fig.

2(b)). The physical cause of the SDR is still under discussion. Possible origins include hydrogen-induced recombination centres, as PECVD-SiN_x contains large amounts of hydrogen, or stress-induced defects due to the different thermal expansion coefficients of SiN_x and Si. Interestingly, we were able to show that the modelling of the $S_{eff}(\Delta n)$ dependence on Al_2O_3-passivated silicon wafers also requires the assumption of an SDR, although this SDR seems to be less deep than in the case of SiN_x [8]. The negative Q_f in the Al_2O_3 layer, however, reverses the $S_{eff}(\Delta n)$ behaviour concerning the conductance type. As now an accumulation layer is formed on *p*-type silicon, a negligible $S_{eff}(\Delta n)$ dependence is observed at the Al_2O_3/*p*-Si interface and a more pronounced $S_{eff}(\Delta n)$ dependence is observed at the Al_2O_3/*n*-Si interface (triangles down in Figs. 2 (a) and (b)). Concerning the absolute S_{eff} values, however, we observe lower S_{eff} values using ALD-Al_2O_3 compared to PECVD-SiN_x on *p*- as well as on *n*-type Si (see Figs. 2 (a) and (b)).

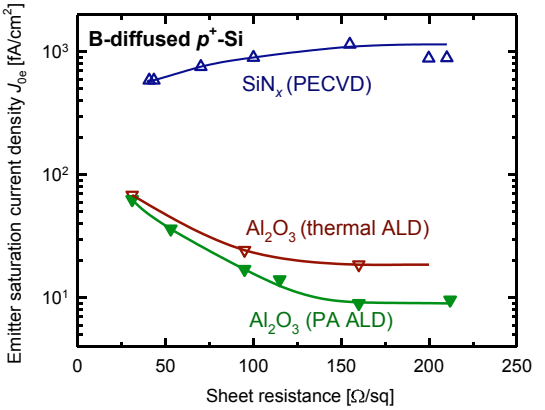

Fig. 3. Measured emitter saturation current densities J_{0e} as a function of the sheet resistance of boron-diffused p^+ emitters. SiN_x data were taken from Ref. [23]. The lines are guides to the eye.

It has been shown that Al_2O_3 also provides an excellent and stable level of surface passivation on boron-diffused p^+-emitters [5]. Figure 3 shows a comparison of measured emitter saturation current densities J_{0e} of boron-diffused p^+ emitters of varying sheet resistances passivated by PA-ALD and thermal ALD-Al_2O_3 and in comparison with PECVD-SiN_x (SiN_x data were taken from Ref. [23]). Independent of the particular ALD technique used, very low J_{0e} values of ~20 fA/cm^2 (corresponding to a limiting open-circuit voltage of $V_{oc.limit}$ = 740 mV) are obtained for a sheet resistance of around 90 Ω/sq. In the same sheet resistance range, the J_{0e} of the SiN_x-passivated emitter amounts to 900 fA/cm^2 (corresponding to a limiting V_{oc} of only 640 mV). It has to be mentioned that optimised high-temperature treatments and special cleaning sequences to improve the SiN_x passivation quality on p^+-emitters have recently been successfully developed [24]. It is a common misbelief that the high positive Q_f within the SiN_x layer explains that SiN_x passivates phosphorus-diffused n^+ emitters quite well, but boron-diffused p^+ emitters to a significantly lesser extent. From simulation studies it has been shown that the high positive Q_f in the SiN_x layer is not sufficient to explain the poor surface passivation of p^+ emitters [9]. The main cause for the unsatisfactory passivation quality of PECVD-SiN_x on boron-diffused p^+ emitters is in fact most likely the highly asymmetric capture cross sections for electrons and holes of the interface states [9]. From this it can be concluded that the fact that Al_2O_3 passivates p^+ emitters extremely well cannot be explained by the high negative Q_f alone either, but additionally requires favourable capture cross section values of the Al_2O_3/Si interface states.

3. Industrially suitable Al_2O_3 deposition techniques

In a conventional ALD process, the separation of the two half-reactions is implemented by an alternate dosing of the process gases, which are usually trimethyl aluminium (TMA) and H_2O for thermal ALD or instead of H_2O a remote oxygen plasma for PA-ALD. Exposure times of only a few milliseconds are sufficient to ensure complete saturation of the growth surface. In between both precursor doses, however, the reactor chamber is purged with an inert gas and subsequently pumped to remove the residual process gas and reaction products. To prevent parasitic CVD processes and to ensure a true ALD process, pumping times of the order of a few seconds are required, severely limiting the growth rate to approximately 2 nm/min. This makes conventional ALD unsuitable for high-throughput industrial solar cell production. Recently, Poodt *et al.* [25] proposed a high-rate fast ALD concept based on spatially separated ALD ('*spatial ALD*'), enabling *high deposition rates* of 70 nm/min. In contrast to the conventional sequential separation, both half-reactions are *spatially* separated, thus eliminating the need for intermediate pumping steps. In a first proof-of-principle tool developed at TNO [25], the spatial separation was achieved by rotating the wafer underneath a round reactor head incorporating gas inlets for TMA and water vapour, separated by gas bearing planes formed by a flow of pressurised nitrogen. Since both reaction zones are sealed off by nitrogen flow, any unintentional interaction of the process gases is prevented and the deposition can be performed under atmospheric conditions, an additional advantage concerning the industrial applicability. We have recently demonstrated that using Al_2O_3 deposited by high-rate spatial ALD the same level of excellent surface passivation as obtained by conventional thermal ALD is achieved on *p*- and *n*-type silicon wafers [26]. As can be seen from Fig. 4 (a), S_{eff} values below 10 cm/s are achieved on 1-Ωcm *p*-type silicon over a broad injection range between 10^{13} and 10^{15} cm^{-3} by high-rate spatial ALD. High-throughput (up to 3,000 wafers per hour) reactors based on the spatial ALD approach are currently under development at two different companies, namely SoLayTec and Levitech, and will be commercially available in the near future with the extra option of an additional gas bearing at the wafer back side, thus enabling double-floating wafer transport in a reciprocating manner or in a single direction.

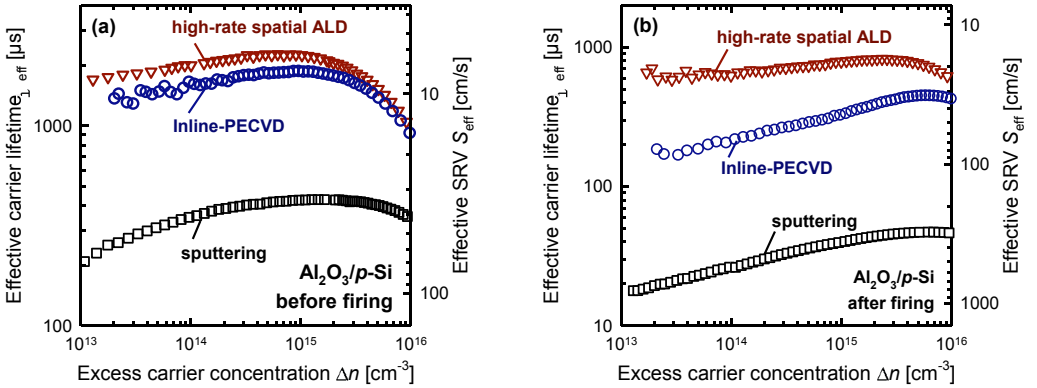

Fig. 4. Effective lifetime τ_{eff} and corresponding effective SRV S_{eff} as a function of the excess carrier concentration Δn measured on 1-Ωcm *p*-type FZ-Si (a) before and (b) after firing in an industrial conveyor-belt furnace (data taken from Ref. [30]).

Recently, two other techniques were demonstrated to be suitable for depositing surface-passivating Al_2O_3 layers. Plasma-enhanced chemical vapour deposition (PECVD) [27, 28] was shown to provide SRVs of 10 cm/s on 1-Ωcm *p*-type FZ-Si [28], whereas reactive sputtering [29] on comparable material

resulted in SRVs down to 55 cm/s. In a recent contribution [30], the passivation quality of Al_2O_3 deposited by inline-PECVD (Roth&Rau, SiNA) and by rf magnetron sputtering (homemade setup at ANU) was studied. The sputtering uses an aluminium target, which is reactively sputtered in an O_2/Ar atmosphere [29], while the PECVD uses TMA and nitrous oxide as process gases. Figure 4(a) compares the effective lifetimes measured on 1-Ωcm *p*-type FZ-Si wafers passivated by Al_2O_3 films deposited using the three, in our opinion, most promising industrial Al_2O_3 deposition techniques: (i) high-rate spatial ALD, (ii) PECVD, and (iii) rf magnetron sputtering. The direct lifetime comparison in Fig. 4(a) shows that both spatial ALD and PECVD provide S_{eff} values < 10 cm/s, clearly outperforming the sputtered Al_2O_3. Nevertheless, the sputtered Al_2O_3 passivation layer results in S_{eff} values between 35 and 70 cm/s in the relevant injection range, which would be still sufficient for the next generation of industrial high-efficiency solar cells.

A very important property concerning the industrial applicability of Al_2O_3 is the stability of the surface passivation during firing. Hence, we have annealed the lifetime samples of Fig. 4(a) in an industrial infrared conveyor-belt furnace at a measured peak temperature of ~800°C for a few seconds. Figure 4(b) shows the injection-dependent lifetimes and corresponding surface recombination velocities measured after firing. The Al_2O_3 deposited by high-rate spatial ALD shows clearly the best firing stability, providing SRVs of ~20 cm/s after firing over the entire relevant injection range. The Al_2O_3 layer deposited by inline-PECVD also results in a good passivation quality after firing, providing S_{eff} values between 30 and 80 cm/s in the relevant injection range. The sputtered Al_2O_3 shows the strongest increase in the surface recombination after firing, leading to SRVs between 300 and 800 cm/s. Obviously, the sputtered Al_2O_3 needs further optimisation, while the PECVD-Al_2O_3 and in particular the spatial ALD-Al_2O_3 layers can directly be implemented into an industrial-type screen-printing solar cell process.

As we have demonstrated recently, the firing stability of the Al_2O_3 layers can be further improved by adding a hydrogen-rich PECVD-SiN_x capping layer [31, 32]. Using such Al_2O_3/SiN_x stacks we have in fact achieved effective SRVs of ≤ 10 cm/s after firing for Al_2O_3 layers deposited by PA-ALD as well as by thermal ALD. An excellent firing stability of Al_2O_3/SiN_x stacks was also reported by other researchers [33, 34]. Al_2O_3/SiN_x stacks are hence perfectly suited for the surface passivation of industrial screen-printed silicon solar cells.

4. Application to solar cells

High cell efficiencies (> 20%) using Al_2O_3 surface passivation had first been realized on *p*-type [4] as well as *n*-type silicon [35] wafers only briefly after the very promising first lifetime results had been published [2, 3, 5]. Table 1 shows a summary of the currently highest efficiencies achieved on *p*-type silicon wafers using a PERC cell structure, where the rear is passivated by Al_2O_3 deposited by different deposition techniques such as ALD, PECVD and sputtering. All cell parameters listed in Table 1 were independently confirmed. The efficiencies achieved on 4 cm^2 lab-type cells using ALD [36] and PECVD [28] are practically identical within the measurement uncertainty (cells P1 and P2 in Table 1). For the best cell with 21.7% efficiency [36] we have implemented an additional contact passivation underneath the front Al grid. This contact passivation is realised by a PA-ALD-AlO_x layer, where only two ALD cycles were applied, which resulted in a 12 mV increase in V_{oc} [36]. Cell P3 with a sputtered AlO_x rear passivation still achieves an efficiency of 20.1% [30] despite the simple sputtering deposition technique [29], which does not require any expensive gases such as TMA. Importantly, cells P1 – P3 in Table 1 did not undergo any firing step, which is a standard high-temperature process step in the industrial solar cell production. Hence, at ISFH we have developed an industrial-type PERC solar cell with fully screen-

printed and fired contacts on 12.5×12.5 cm^2 pseudo-square boron-doped *p*-type Cz-Si [37]. This cell P4 shows the so far best cell results with an Al_2O_3/SiN_x rear passivation on large-area wafers. The 19.0% efficient cell P4 does, however, not include any selective emitter at the front and has a non-optimised rear geometry of the local laser contact openings [37]. Hence, we estimate an efficiency limit exceeding 20% for an optimised cell of this type including a selective emitter [38].

Table 1. *p*-type silicon PERC solar cells with Al_2O_3 rear passivation. The Al_2O_3 is deposited by different deposition techniques such as ALD, PECVD and sputtering. All cell parameters were independently confirmed at FhG-ISE CalLab.

	Metallisation	Rear passivation	Area [cm^2]	V_{oc} [mV]	J_{sc} [mA/cm^2]	*FF* [%]	η [%]	Ref.
P1	Shadow-mask evaporated Al	ALD-Al_2O_3/PECVD-SiN_x	4	673	40.3	79.9	21.7	[36]
P2	Evap. Ti/Pd/Ag, photolithography	PECVD-AlO_x	4	684	39.4	79.8	21.5	[28]
P3	Shadow-mask evaporated Al	Sputtered AlO_x	4	651	39.1	79.1	20.1	[30]
P4	Screen-printed front and rear	ALD-Al_2O_3/PECVD-SiN_x	149	652	38.9	75.1	19.0	[37]

Table 2 summarises some of the best cell results achieved so far on high-lifetime *n*-type silicon, where the boron-diffused p^+ emitter has been passivated by ALD-Al_2O_3/PECVD-SiN_x stacks. Cell N1 is a passivated emitter and rear, locally diffused (PERL) cell, where the rear is passivated by high-temperature grown SiO_2 and a local phosphorus diffusion was implemented to create the local back surface field. Due to the excellent Al_2O_3 passivation of the p^+ front emitter [5, 35], this cell achieves a very high V_{oc} of 705 mV and the best efficiency of 23.9% [39]. Cell N2 is a back-contact emitter-wrap-through (EWT) solar cell, where the boron-diffused p^+ emitter covers the entire front and a large part of the cell rear [40]. Hence, the quality of the applied Al_2O_3/SiN_x passivation scheme is of utmost importance. The achieved V_{oc} of 661 mV and the efficiency of 21.6% [40] of this EWT cell on *n*-type Cz-Si clearly reveal the high potential of the Al_2O_3 passivation for this cell type. Table 2 also includes a large-area cell with boron-diffused p^+ front emitter and a printed, fired and electroplated front contact grid [41]. The entire rear was phosphorus-diffused and metallised by evaporated aluminium. The front of this 19.6% [41] efficient *n*-type cell was passivated by a firing-stable Al_2O_3/SiN_x stack. The cell results shown in Tables 1 and 2 prove that Al_2O_3/SiN_x stacks are perfectly suited for the next generation of industrial high-efficiency solar cells on *p*- as well as on *n*-type silicon.

Table 2. *n*-type silicon solar cells with Al_2O_3/SiN_x-passivated boron-diffused p^+-emitter. The parameters of cells N1 and N2 were independently confirmed at FhG-ISE CalLab.

	Cell structure	Area [cm^2]	V_{oc} [mV]	J_{sc} [mA/cm^2]	*FF* [%]	η [%]	Ref.
N1	PERL; rear: SiO_2-passivated, local n^+	4	705	41.1	82.5	23.9	[35,39]
N2	EWT; locally contacted SiO_2-passivated n^+	4	661	40.4	80.8	21.6	[40]
N3	Front grid: printed, fired, plated; rear: evaporated Al	141	649	38.5	78.3	19.6	[41]

5. Conclusions

Lifetime as well as solar cell results demonstrate the enormous potential of Al_2O_3 as a surface-passivating dielectric layer for the next generation of industrial silicon solar cells on *p*- as well as *n*-type silicon wafers. The question remains open what will be the best suited deposition technique and on what

timescale it can be transferred to industry. The highest film quality is currently realised by means of PA-ALD, which is in its current form not able to deliver the throughput required in a solar cell production line. We have hence evaluated three different deposition techniques which are in principle suitable for the required throughput, namely high-rate spatial ALD, inline-PECVD, and sputtering. As large-area inline-PECVD systems are already available on the market, PECVD seems to be the preferred short-term deposition techniques for Al_2O_3. If the firing stability of sputtered Al_2O_3 layers could be further improved (e.g. by using a hydrogen-rich SiN_x capping layer), this could become another option for the short-term. The preferred medium-term and long-term deposition technique might be the ultrafast spatial ALD due to its reduced TMA gas consumption compared to PECVD, the absence of parasitic deposition at the reactor wall and a smaller footprint of the deposition systems currently under development. Also, ALD provides highest-quality pinhole-free Al_2O_3 films and allows conformal film deposition, which might prove useful for advanced solar cell concepts such as back-contact EWT cells.

Acknowledgements

Funding was provided by the State of Lower Saxony and the German Ministry for the Environment, Nature Conservation and Nuclear Safety (BMU) under contract number 0325050 (“ALD”).

References

[1] Hezel R, Jaeger K. Low-temperature surface passivation of silicon for solar cells. *J. Electrochem. Soc.* 1989; **136**: 518.
[2] Agostinelli G, Delabie A, Vitanov P, Alexieva Z, Dekkers HFW, De Wolf S, Beaucarne G. Very low surface recombination velocities on p-type silicon wafers passivated with a dielectric with fixed negative charge. *Sol. Energy Mat. Sol. Cells* 2006; **90**: 3438.
[3] Hoex B, Heil SBS, Langereis E, van de Sanden MCM, Kessels WMM. Ultralow surface recombination of *c*-Si substrates passivated by plasma-assisted atomic layer deposited Al_2O_3. *Appl. Phys. Lett.* 2006; **89**: 042112.
[4] Schmidt J, Merkle A, Brendel R, Hoex B, van de Sanden MCM, Kessels WMM. Surface passivation of high-efficiency silicon solar cells by atomic-layer-deposited Al_2O_3. *Prog. Photovolt. Res. Appl.* 2008; **16**: 461.
[5] Hoex B, Schmidt J, Bock R, Altermatt PP, van de Sanden MCM, Kessels WMM. Excellent passivation of highly doped p-type Si surfaces by the negative-charge-dielectric Al_2O_3. *Appl. Phys. Lett.* 2007; **91**: 112107.
[6] Bock R, Schmidt J, Mau S, Hoex B, Brendel R. The ALU+ concept: n-type silicon solar cells with surface-passivated screen-printed aluminium-alloyed rear emitter. *IEEE Trans. Electron Devices* 2010; **57**: 1966.
[7] Hoex B, Gielis JJH , van de Sanden MCM, Kessels WMM. On the *c*-Si surface passivation mechanism by the negative-charge-dielectric Al_2O_3. *J. Appl. Phys.* 2008; **104**: 113703.
[8] Steingrube S, Altermatt PP, Zielke D, Werner F, Schmidt J, Brendel R. Reduced passivation of silicon surfaces at low injection densities caused by H-induced defects. *Proc. 25th European Photovoltaic Solar Energy Conf., Valencia, Spain*, Munich: WIP; 2010, p. 1748-54.
[9] Altermatt PP, Plagwitz H, Bock R, Schmidt J, Brendel R, Kerr MJ, Cuevas A. The surface recombination velocity at boron-doped emitters: comparison between various passivation techniques. *Proc. 21st European Photovoltaic Solar Energy Conf., Dresden, Germany*, Munich: WIP; 2006, p. 647-50.
[10] Cuevas A, Kerr MJ, Schmidt J. Passivation of crystalline silicon using silicon nitride. *Proc. 3rd World Conf. Photovoltaic Solar Energy Conversion, Osaka, Japan*; 2003, p. 913-8.
[11] Elmiger JR, Kunst M. Investigation of charge carrier injection in silicon nitride/silicon junctions. *Appl. Phys. Lett.* 1996; **69**: 517.
[12] Aberle AG, Glunz SW, Warta W. Impact of illumination level and oxide parameters on Shockley-Read-Hall recombination at the Si-SiO_2 interface. *J. Appl. Phys.* 1992; **71**: 4422.
[13] Terlinden NM, Dingemans G, van de Sanden MCM, Kessels WMM. Role of field-effect on c-Si surface passivation by ultrathin (2–20 nm) atomic layer deposited Al_2O_3. *Appl. Phys. Lett.* 2010; **96**: 112101.
[14] Werner F, Veith B, Zielke D, Kühnemund L, Tegenkamp C, Seibt M, Brendel R, Schmidt J. Electronic and chemical properties of the c-Si/Al_2O_3 interface. *J. Appl. Phys.* 2011; **109**: 113701.
[15] Warren WL, Rong FC, Poindexter EH, Gerardi GJ, Kanicki J. Structural identification of the silicon and nitrogen dangling-bond centres in amorphous silicon nitride. *J. Appl. Phys.* 1991; **70**: 346.

[16] Schmidt J, Aberle AG. Carrier recombination at silicon-silicon nitride interfaces fabricated by plasma-enhanced chemical vapour deposition. *J. Appl. Phys*. 1999; **85**: 3626.
[17] Matsunaga K, Tanaka T, Yamamoto T, Ikuhara Y. First-principles calculations of intrinsic defects in Al_2O_3. *Phys. Rev. B* 2003;**68**: 085110.
[18] Dauwe S, Schmidt J, Metz A, Hezel R. Fixed charge density in silicon nitride films on crystalline silicon surfaces under illumination. *Proc. 29th IEEE Photovoltaic Specialists Conf., New Orleans, USA* , New York: IEEE; 2002, p.162-5.
[19] Girisch RBM, Mertens RP, de Keersmaecker RF. Determination of the Si-SiO_2 interface recombination parameters using a gate-controlled point-junction diode under illumination. *IEEE Trans. Electron Dev.* 1988; **35**: 203.
[20] Dauwe S. Low-temperature rear surface passivation of crystalline silicon solar cells [PhD thesis]. University of Hanover, 2004.
[21] Schmidt J, Moschner JD, Henze J, Dauwe S, Hezel R. Recent progress in the surface passivation of silicon solar cells using silicon nitride. *Proc. 19th European Photovoltaic Solar Energy Conf., Paris, France*, Munich: WIP; 2004, p. 391-6.
[22] Steingrube S, Altermatt PP, Steingrube DS, Schmidt J, Brendel R. Interpretation of recombination at c-Si/SiN_x interfaces by surface damage. *J. Appl. Phys*. 2010; **108**: 014506.
[23] Kerr MJ. Surface, emitter and bulk recombination in silicon and development of silicon nitride passivated solar cells [PhD thesis]. Australian National University, 2002.
[24] Chen FW, Li T, Cotter JE. Passivation of boron emitters on n-type silicon by plasma-enhanced chemical vapour deposited silicon nitride. *Appl. Phys. Lett.* 2006; **88**: 263514.
[25] Poodt P, Lankhorst A, Roozeboom F, Spee K, Maas D, Vermeer A, High-speed spatial atomic layer deposition of aluminium oxide layers for solar cell passivation. *Advanced Materials* 2010; **22**: 3564.
[26] Werner F, Veith B, Tiba V, Poodt P, Roozeboom F, Brendel R, Schmidt J. Very low surface recombination velocities on p- and n-type c-Si by ultrafast spatial atomic layer deposition of aluminium oxide. *Appl. Phys. Lett.* 2010; **97**: 162103.
[27] Miyajima S, Irikawa J, Yamada A, Konagai M. Hydrogenated aluminium oxide films deposited by plasma enhanced chemical vapour deposition for passivation of p-type crystalline silicon. *Proc. 23rd Photovoltaic Solar Energy Conf., Valencia, Spain*, Munich: WIP; 2008, p. 1029.
[28] Saint-Cast P, Kania D, Hofmann M, Benick J, Rentsch J, Preu R. Very low surface recombination velocity on p-type c-Si by high-rate plasma-deposited aluminium oxide. *Appl. Phys Lett.* 2009; **95**: 151502.
[29] Li TT, Cuevas A. Effective surface passivation of crystalline silicon by rf sputtered aluminium oxide. *Phys. Status Solidi RRL* 2009; **3**: 160.
[30] Schmidt J, Werner F, Veith B, Zielke D, Bock R, Tiba V, Poodt P, Roozeboom F, Li A, Cuevas A, Brendel R. Industrially relevant Al_2O_3 deposition techniques for the surface passivation of Si solar cells. *Proc. 25th European Photovoltaic Solar Energy Conf., Valencia, Spain* (WIP, Munich, 2010), p. 1130-1133.
[31] Schmidt J, Veith B, Brendel R. Effective surface passivation of crystalline silicon using ultrathin Al_2O_3 films and Al_2O_3/SiN_x stacks. *Phys. Status Solidi RRL* 2009; **3**: 287.
[32] Veith B, Werner F, Zielke D, Brendel R, Schmidt J. Comparison of the thermal stability of single Al_2O_3 layers and Al_2O_3/SiN_x stacks for the surface passivation of silicon. *Energy Procedia* 2011; in press.
[33] Benick J, Richter A, Hermle M, Glunz SW. Thermal stability of the Al_2O_3 passivation on p-type silicon surfaces for solar cell applications. *Phys. Status Solidi RRL* 2009; **3**: 233.
[34] Dingemans G, Engelhart P, Seguin R, Einsele F, Hoex B, van de Sanden MCM, Kessels WMM. Stability of Al_2O_3 and Al_2O_3/*a*-SiN_x:H stacks for surface passivation of crystalline silicon. *J. Appl. Phys.* 2009; **106**: 114907.
[35] Benick J, Hoex B, van de Sanden MCM, Kessels WMM, Schultz O, Glunz SW. High-efficiency n-type Si solar cells on Al_2O_3-passivated boron emitters. *Appl. Phys. Lett.* 2008; **92**: 253504.
[36] Zielke D, Petermann JH, Werner F, Veith B, Brendel R, Schmidt J. Contact passivation in silicon solar cells using atomic-layer-deposited aluminium oxide layers. *Phys. Status Solidi RRL* 2011; **5**: 298.
[37] Gatz S, Hannebauer H, Hesse R, Werner F, Schmidt A, Dullweber T, Schmidt J, Bothe K, Brendel R. 19.4%-efficient large-area fully screen-printed silicon solar cells. *Phys. Status Solidi RRL* 2011; **5**: 147.
[38] Dullweber T, Gatz S, Hannebauer H, Falcon T, Hesse R, Schmidt J, Brendel R. Towards 20% efficient large-area screen-printed rear-side-passivated silicon solar cells. *Prog. Photovolt. Res. Appl.* 2011, submitted.
[39] Glunz SW, Benick J, Biro D, Bivour M, Hermle M, Pysch D, Rauer M, Reichel C, Richter A, Rüdiger M, Schmiga C, Suwito D, Wolf A, Preu R. n-type silicon – enabling efficiencies >20% in industrial production. *Proc. 35th IEEE Photovoltaic Specialists Conf., Honolulu, USA* , New York: IEEE; 2010, p. 50-6.
[40] Kiefer F, Ulzhöfer C, Brendemühl T, Harder NP, Brendel R, Mertens V, Bordihn S, Peters C, Müller JW. High-efficiency n-type emitter-wrap-through silicon solar cells. *IEEE Journal of Photovoltaics* 2011, submitted.
[41] Richter A, Henneck S, Benick J, Hörteis M, Hermle M, Glunz SW. Firing stable Al_2O_3/SiN_x layer stack passivation for the front side boron emitter of n-type silicon solar cells. *Proc. 25th European Photovoltaic Solar Energy Conf., Valencia, Spain* (WIP, Munich, 2010), p. 1453-9.